Check for updates

Gas Separation Hot Paper

How to cite: *Angew. Chem. Int. Ed.* **2022**, *61*, e202208134
International Edition: doi.org/10.1002/anie.202208134
German Edition: doi.org/10.1002/ange.202208134

One-Step Ethylene Purification from Ternary Mixtures in a Metal–Organic Framework with Customized Pore Chemistry and Shape

Qi Ding[+], *Zhaoqiang Zhang*[+], *Yulong Liu, Kungang Chai, Rajamani Krishna, and Sui Zhang**

Abstract: Adsorptive separation is an energy-efficient technology for the separation of C2 hydrocarbons. However, it remains a critical problem to directly produce high-purity C_2H_4 from ternary $C_2H_2/C_2H_4/C_2H_6$ mixtures by simultaneously trapping C_2H_2 and C_2H_6. Herein, we report the one-step C_2H_4 purification from the ternary mixture by a metal–organic framework Zn(ad)(int) (ad = adeninate; int = isonicotinate). The material combines dense heterocyclic rings and accessible uncoordinated O atoms as strong binding sites for C_2H_6 and C_2H_2. Its spindle-like cage exhibits an interesting shape matching with the targeted molecules, affording Zn(ad)(int) not only high separation selectivity for C_2H_6/C_2H_4 and C_2H_2/C_2H_4, but also excellent gas capacity. Breakthrough experiments show that polymer-grade C_2H_4 can be separated from the ternary mixtures with a record productivity of 1.43 mmol g^{-1}. In situ powder X-ray diffraction and Fourier transform infrared spectrum analyses further provide deep insights into the separation mechanism.

Introduction

Ethylene (C_2H_4) is a prime building block for the synthesis of polyethylene and many other organic chemicals in the petrochemical industry.[1] By 2020, the worldwide annual production of C_2H_4 had reached 201 Mt, exceeding that of any other fundamental chemicals. C_2H_4 is usually obtained by the thermal cracking of hydrocarbons, where ethane (C_2H_6) and acetylene (C_2H_2) are inevitably co-produced as byproducts. However, a trace amount of C_2H_2 (1000–5000 ppm) would poison the catalysts for C_2H_4 polymerization and even lead to an explosion; furthermore, C_2H_6 can also compromise the polymer production efficiency,[2] highlighting the necessity of isolating C_2H_4 from C2 mixtures with high efficiency. In a typical sequential separation procedure, C_2H_2 is firstly eliminated from the C2 mixtures via catalytic hydrogenation under high pressure and temperatures; then, C_2H_6 is separated by energy-intensive cryogenic distillations under −25 °C and up to 22 bar.[3] The purification of C_2H_4 together with propylene accounts for nearly 0.3 % of the global energy consumption,[4] suggesting novel energy-saving separation methods are strongly demanded.

The burgeoning progress in advanced porous materials has greatly spurred the energy-efficient adsorptive separation technology on the purification of many industrially important gases.[5] Thus far, the high-efficiency adsorptive separations of binary C2 mixtures (C_2H_2/C_2H_4 or C_2H_6/C_2H_4) have been realized with various materials like metal–organic frameworks (MOFs),[6] covalent organic framework (COFs),[7] zeolites,[8] carbon materials,[9] and porous organic cages.[10] Comparably, versatile materials with the ability to simultaneously capture C_2H_2 and C_2H_6 from ternary $C_2H_2/C_2H_4/C_2H_6$ mixtures are more desirable, which means that high-purity C_2H_4 can be cost-efficiently obtained with remarkably reduced adsorption–desorption cycles. However, the design of C_2H_2/C_2H_6-selective materials is still in its infancy stage and challenged by the opposite binding preference of C_2H_2 and C_2H_6. Since C_2H_2 has a higher acidity (pK_a: 26 vs. 45) and larger quadrupole moment (3.0×10^{-26} vs. 1.5×10^{-26} esu cm^2) than C_2H_4 (Table S1), the preferential trap of C_2H_2 over C_2H_4 is usually achieved with materials constructed from highly polar groups (e.g., unsaturated metal sites and inorganic anion pillars) that show strong electrostatic interactions with the guests;[11] the selective adsorption of C_2H_6 over C_2H_4 (polarizability: 44.7×10^{-25} vs. 42.5×10^{-25} cm^3), contrarily, is often favored by low-polarity functional groups (e.g., aromatic rings and aliphatic chains) that exhibit relatively weak van der Waals (vdW) interaction.[12] Such an inherent contradiction implies that incorporating high- and low-polarity functional groups into the same pore system, meanwhile finely tuning their spatial distributions to allow the effective recognition of C_2H_2 and C_2H_6, respectively, is a vital starting point. This puts forward a high demand on the precise control of surface chemistry and pore geometry, hindering most C_2H_2/C_2H_6-selective materials from being highly selective for C_2H_2/C_2H_4 and C_2H_6/C_2H_4 at the same time.[13] For example, the benchmark

[*] Dr. Q. Ding,[+] Dr. Z. Zhang,[+] Prof. S. Zhang
Department of Chemical and Biomolecular Engineering, National University of Singapore
4 Engineering Drive 4, Singapore, 117585 (Singapore)
E-mail: chezhasu@nus.edu.sg

Y. Liu, Prof. K. Chai
School of Chemistry and Chemical Engineering, Guangxi Key Laboratory of Petrochemical Resource Processing and Process Intensification Technology, Guangxi University
Nanning 530004 (P. R. China)

Prof. R. Krishna
Van't Hoff Institute for Molecular Sciences
University of Amsterdam
Science Park 904, 1098 XH Amsterdam (The Netherlands)

[+] These authors contributed equally to this work.

© 2022 Wiley-VCH GmbH

MOFs, UiO-67-$(NH_2)_2$[13e] and Azole-Th-1,[13h] show high efficiency for the separation of C_2H_2/C_2H_4 and C_2H_6/C_2H_4, respectively, whereas their adsorption selectivity towards C_2H_6 (1.7) and C_2H_2 (1.09) are modest. Apart from that, the lack of strong binding site emerges as another important reason for the undesirable C_2H_6 selectivity, and it also causes an unsatisfactory capture ability for low-level C_2H_6 as can be commonly observed among the current C_2H_2/C_2H_6-selective materials ($<25\ cm^3\,g^{-1}$ at 298 K and 0.1 bar). The insufficient gas trapping ability is unfavorable by considering that the C2 fraction obtained from cracked gas usually contains a small portion of C_2H_6 (ca. 6–10 %).[14] Consequently, novel C_2H_2/C_2H_6-selective materials with both significantly improved separation selectivity and excellent gas capacity are still highly expected to enhance the purification of C_2H_4.

Herein, we report the one-step purification of C_2H_4 from ternary $C_2H_2/C_2H_4/C_2H_6$ mixture by a MOF Zn(ad)(int) (ad = adeninate; int = isonicotinate) with customized pore chemistry and shape. The material well combines dense polar heterocyclic rings and accessible uncoordinated O atoms as strong binding acceptors for C_2H_6 and C_2H_2. Meanwhile, the featured spindle-like molecular cage exhibits an interesting shape matching with the target gas molecules, promoting both C_2H_6 and C_2H_2 to be effectively recognized. Zn(ad)(int) shows not only outstanding selectivities for C_2H_6/C_2H_4 and C_2H_2/C_2H_4 mixtures (2.4 and 1.61), but also an excellent trapping ability for low-level C_2H_2 and C_2H_6 (33.4 and 41.0 $cm^3\,g^{-1}$ at 298 K and 0.1 bar, respectively). Breakthrough experiments indicate that polymer-grade (99.9 %) C_2H_4 can be separated from ternary $C_2H_2/C_2H_4/C_2H_6$ mixture with a record productivity of 1.43 $mmol\,g^{-1}$, presenting Zn(ad)(int) as a top-performing C_2H_2/C_2H_6-selective material. In situ powder X-ray diffraction (PXRD) and Fourier transform infrared spectroscopy (FTIR) further provide important insights into the separation mechanism at the molecular level.

Results and Discussion

Zn(ad)(int) was synthesized by a hydrothermal method with zinc nitrate, isonicotinic acid, and adenine as the reagents.[15] Its structure contains 1D spiral chains made of Zn nodes and axial-symmetrically arranged ad (Figure 1a). The other ligand, int, behaves as a bridge that holds two spiral chains together via Zn–N and Zn–O coordination bonds (Figure 1a), leading to the 3D porous structure of Zn(ad)(int) (Figure 1b) with spindle-like cages inside (aperture size: 7.1 Å, Figure 1c), which may exhibit distinct degrees of shape matching towards the C2 molecules (oblate C_2H_6, planar C_2H_4, and linear C_2H_2). The surface of the cage is mostly surrounded by heterocyclic rings carrying abundant N atoms. Meanwhile, the partial chelation of carboxyl group with the Zn node allows the formation of uncoordinated O atoms (highlighted by ball mode in Figure 1c) that are distributed at the narrow conner of the cage and remain accessible for small molecules. According to the mapping of electrostatic potential (Figure 1d), these heterocyclic rings are slightly polarized with π-clouds enriched around the electronegative N atoms. This indicates that they may exhibit a stronger ability to interact with C_2H_6 compared to nonpolar benzene rings that are commonly utilized for inverse C_2H_6/C_2H_4 separation. Moreover, the uncoordinated O atoms with lone-pair electrons possess even higher electron density, presenting them as potential strong H-bond acceptors for acidic C_2H_2. We speculated that the combination of customized pore chemistry and intriguing pore shape may afford Zn(ad)(int) a dramatic ability to capture C_2H_6 and C_2H_2.

Prior to further investigation, Zn(ad)(int) was characterized by PXRD analysis (Figure S1), where the consistency between experimental and simulated patterns confirms that the product is in high phase purity. Its permanent porosity is verified by N_2 adsorption isotherm at 77 K (Figure S2) with a Brunauer–Emmett–Teller (BET) surface area of 617 $m^2\,g^{-1}$ and pore size of ≈0.8 nm. Further stability tests show that Zn(ad)(int) exhibits a high decomposition temperature of ≈310 °C (Figure S3). Its crystalline structure can be well retained after exposure to air for half a year or soaked in water for three days (Figure S1), which is favorable for industrial application.

The pure-component adsorption isotherms of C2 hydrocarbons were collected at the pressure of up to 1 bar. At 273, 298, and 313 K, the equilibrium uptakes of C_2H_2 and C_2H_6 are higher than C_2H_4 in the whole pressure range (Figure 2a and b, Figure S4), revealing that Zn(ad)(int) can be a potential candidate for the simultaneous trap of C_2H_2 and C_2H_6. Interestingly, unlike most C_2H_2/C_2H_6-selective materials that exhibit limited C_2H_6 uptake at low pressures, the uptakes of C_2H_2 and C_2H_6 on Zn(ad)(int) both increase sharply. At 298 K and 0.1 bar, the uptake of C_2H_6 and C_2H_2 reach 41.0 and 33.4 $cm^3\,g^{-1}$, respectively (Figure 2a). The value for C_2H_6 (41.0 $cm^3\,g^{-1}$) is apparently higher than those of ZJNU-7 (31 $cm^3\,g^{-1}$),[13d] NPU-1 (29 $cm^3\,g^{-1}$),[13f] TJT-100 (27 $cm^3\,g^{-1}$),[2] UiO-67-$(NH_2)_2$ (24.6 $cm^3\,g^{-1}$),[13e] Azole-Th-1 (19 $cm^3\,g^{-1}$),[13h] etc., and to the best of our knowledge, is the highest among all reported C_2H_6/C_2H_4-selective MOFs (Figure 2c).[10,13a,b,d,16] Such a superior gas capacity would endow Zn(ad)(int) with an outstanding capability to trap low-level C_2H_6, which is of particular importance in industry.

The separation selectivities of Zn(ad)(int) for C_2H_6/C_2H_4 and C_2H_2/C_2H_4 were calculated according to ideal adsorbed solution theory (IAST) (Table S2), and excellent values were derived for both mixtures with a wide composition range (Figure 2d). For the C_2H_6/C_2H_4 (10/90) and C_2H_2/C_2H_4 (1/99) mixtures with industrially relevant composition, the separation selectivities are 2.4 and 1.61 at 298 K and 1 bar, respectively. Notably, compared to the reported C_2H_2/C_2H_6-selective materials (Figure 2e), the C_2H_6/C_2H_4 selectivity of Zn(ad)(int) is significantly higher, which outperforms Zn-atz-oba (1.27),[13g] UiO-67-$(NH_2)_2$ (1.7),[13e] NUM-9a (1.62),[13a] and other benchmark materials. Its C_2H_2/C_2H_4 selectivity also exceeds most of the materials like Azole-Th-1 (1.09),[13h] UPC-612 (1.1),[13b] NPU-1 (1.4),[13f] and Zn-atz-oba (1.43).[13g] The combination of high selectivities towards C_2H_6/C_2H_4 and C_2H_2/C_2H_4 mixture is rare, implying that Zn(ad)(int) has a remarkable ability to differentiate the highly similar C2 hydrocarbons.

© 2022 Wiley-VCH GmbH

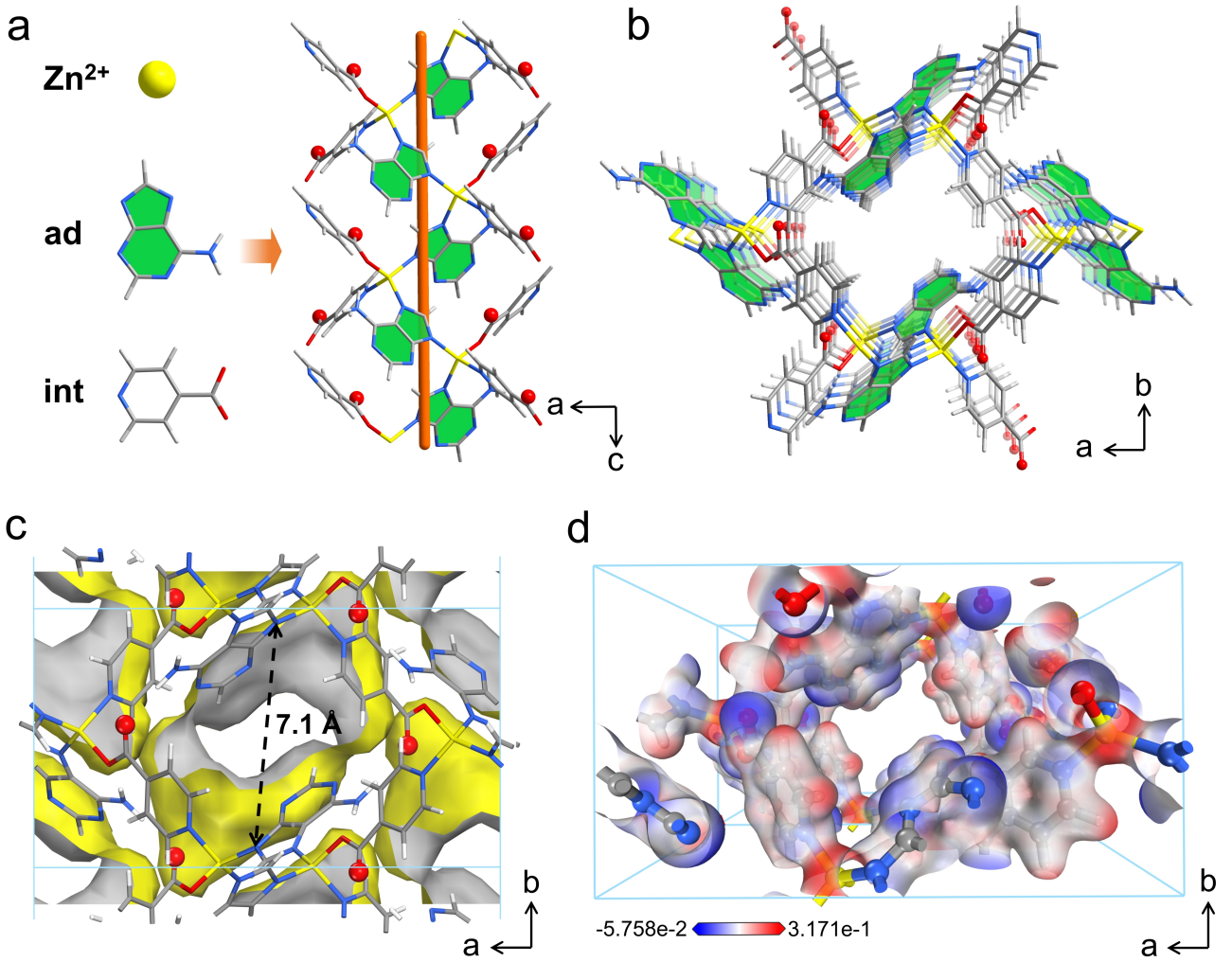

Figure 1. The structure and pore chemistry of Zn(ad)(int). a) Structure of the 1D spiral Zn-ad chain with int ligands hung on the sides (color code: Zn, yellow; C, gray-40%; H, gray-25%; O, red; N, light blue). Uncoordinated O atoms of int are highlighted in ball model for clarity. b) 3D structure of Zn(ad)(int) viewed from c axis. c) Connolly surface of Zn(ad)(int). d) Mapping of the electrostatic potential of Zn(ad)(int) (transparency of 20% is applied for clarity).

The isosteric heat of adsorption (Q_{st}) for different gases were calculated based on their adsorption isotherms at 273, 298, and 313 K by the implementation of Virial equation (Figure S5–S7). At zero loading, the Q_{st} values are 34.7, 28.9, and 33.2 kJ mol^{-1} for C_2H_2, C_2H_4 and C_2H_6, respectively (Figure S8). The higher Q_{st} for C_2H_2 and C_2H_6 compared with C_2H_4 confirm the stronger binding affinities of Zn(ad)-(int) with the former two species, which is consistent with the low-pressure adsorption isotherms. Compared to the existing C_2H_2/C_2H_6-selective materials, Zn(ad)(int) also exhibits a high Q_{st} for C_2H_6 that exceeds most of them (Figure 2f), signifying Zn(ad)(int) has a more powerful binding with C_2H_6.

To gain deep insights into the separation mechanism, in situ PXRD analyses were conducted on gas-loaded Zn(ad)-(int) followed by Rietveld structural refinements to unveil the binding sites of C2 hydrocarbons. Although all these gas molecules are adsorbed near the corner of the spindle-like cage (Figure 3a, Figure S9 and S10), their interaction modes with the pore are much different. The adsorbed C_2H_6 molecule is clearly observed to form multiple C–H···π vdW interactions with three different heterocyclic rings (Figure 3b). Interestingly, the H atoms of C_2H_6 involved in these interactions all contact closely with at least one hetero N atoms coming from these rings, where the H···N distances are 3.00 Å for ring 1, 3.87 and 4.12 Å for ring 2, and 3.15 Å for ring 3. The phenomenon indicates that the N atoms bearing enriched π-cloud have a high tendency to interact with C_2H_6, which is important for the high binding affinity between C_2H_6 and the host framework. Additionally, the C_2H_6 molecule also forms two hydrogen bonds with the uncoordinated O atom of int (H···O = 2.80 Å) and the six-membered ring of ad (ring 4, H···N = 3.03 Å). The fact that C_2H_6 can interact with all the surrounding heterocyclic rings suggest the curve surface of the spindle-shaped cage matches perfectly with the oblate C_2H_6 (Figure 3a), which promotes the precise molecular recognition. Differently, although the adsorbed C_2H_4 also interacts with the material via C–H···O

© 2022 Wiley-VCH GmbH

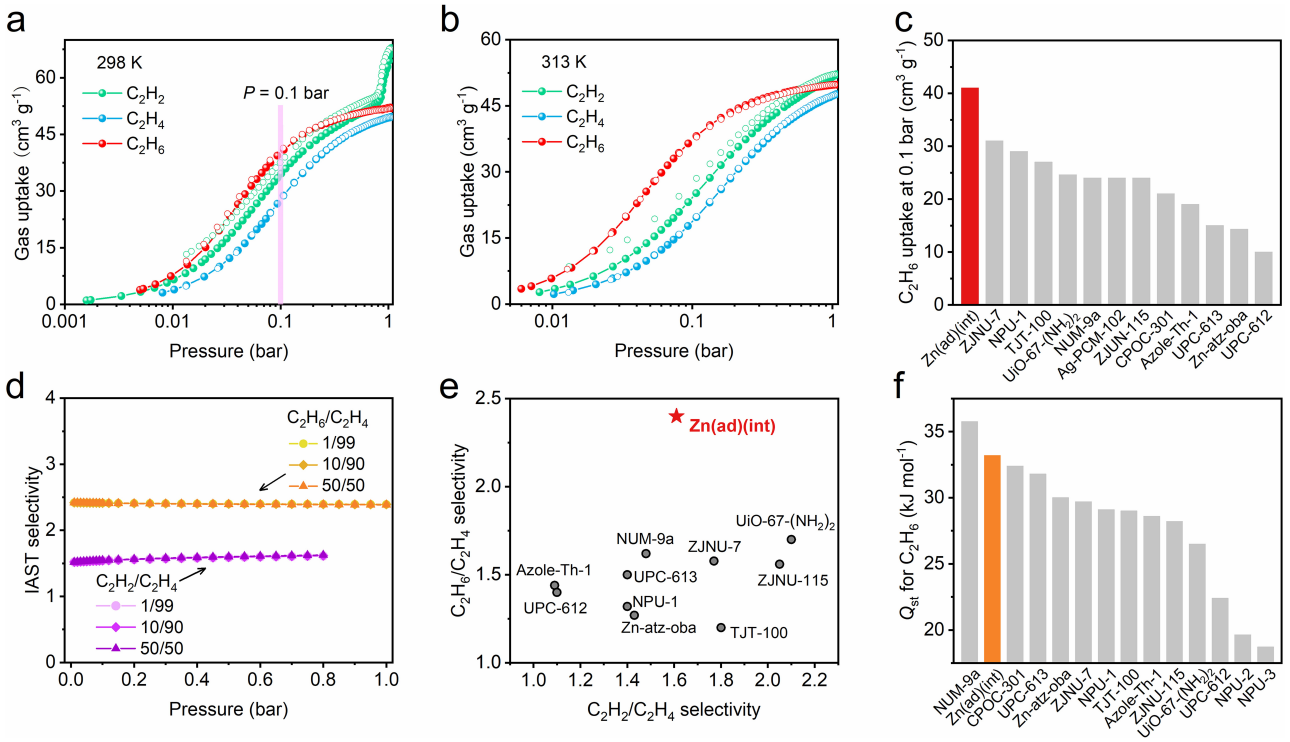

Figure 2. Separation data of Zn(ad)(int). a), b) Adsorption and desorption isotherms of C2 hydrocarbons on Zn(ad)(int) at 298 K and 313 K. The solid and hollow symbols refer to adsorption and desorption branches, respectively. c) A comparison of the C_2H_6 uptake at 0.1 bar among different C_2H_2/C_2H_6-selective materials. d) IAST selectivities of Zn(ad)(int) for C_2H_6/C_2H_4 and C_2H_2/C_2H_4 mixtures with different compositions at 298 K. e) A comparison for the C_2H_6/C_2H_4 and C_2H_2/C_2H_4 selectivities among different C_2H_2/C_2H_6-selective materials. f) A comparison for the Q_{st} of C_2H_6 at zero loading among different C_2H_2/C_2H_6-selective materials.

hydrogen bonding (H···O = 2.63 Å) and C–H···π interactions (H···N = 3.13–3.37 Å, Figure 3c), this molecule fails to interact with ring 3 and ring 4 because its planar shape is less compatible with the curve pore surface (Figure S10). The smaller number of C–H···π interactions with a lack of short H···N distance (shortest H···N distance: 3.00 and 3.13 Å for C_2H_6 and C_2H_4, respectively) implies the weaker vdW interaction between C_2H_4 and the heterocyclic rings. For the adsorbed C_2H_2, the featured linear molecular shape allows it to closely approach the uncoordinated O atom distributed at the narrow corner of the cage (Figure S9), leading to the formation of a strong C–H···O hydrogen bond (Figure 3d) with short H···O distance (2.30 Å) and large ∠C–H···O angle (164°). The other relatively weaker C–H···N hydrogen binding (H···N = 2.47 Å) and π···π stacking with the surrounding heterocyclic rings also help stabilize the adsorbed C_2H_2 molecule. By comparison with the case of C_2H_4 (H···O = 2.63 Å, ∠C–H···O = 149°, Figure 3c), the uncoordinated O atom is evidently more optimal for the binding of C_2H_2 due to its higher acidity compared with C_2H_4, which is a key factor in the highly selective trap of C_2H_2.

We also conducted in situ FTIR analyses to further validate the separation mechanism (Figure S12). After Zn(ad)(int) is loaded with C_2H_2, the formation of a new peak at 1710 cm^{-1} can be clearly seen. This implies a strong binding between C_2H_2 and the uncoordinated O atom, which leads to a change in the vibration of C=O bond in int linker.[17] Moreover, after the sample is loaded with C_2H_6, the occurrence of several new peaks at 1555, 1493, and 1453 cm^{-1} can be observed, which suggests the strong binding between C_2H_6 and the heterocyclic rings that leads to a change in the vibration of C=N and C=C double bonds.[18] These peaks are not found in the spectrum of C_2H_4-loaded Zn(ad)(int) due to the lack of strong host–guest interactions. In all, the results are in good agreement with the in situ PXRD analyses and similarly confirm the essential roles of heterocyclic rings and partially coordinated carboxyl groups in the preferential capture of C_2H_6 and C_2H_2.

To explore the feasibility of Zn(ad)(int) for the separation of gas mixtures, transient breakthrough curves were simulated for C_2H_6/C_2H_4 (10/90 and 50/50) and $C_2H_2/C_2H_6/C_2H_4$ (1/10/89) mixtures at 298 K (Figure 4a and b). The results suggest that clean and sharp separation can be achieved with the three mixtures with high-purity C_2H_4 directly produced. The practical separation ability of Zn(ad)(int) was further validated by dynamic breakthrough experiments. In the separation of binary C_2H_6/C_2H_4 (10/90) mixture (Figure 4c), C_2H_4 quickly broke through the column at 32 min and no noticeable C_2H_6 was detected until its breakthrough time of 52 min. The observed breakthrough times of C_2H_4 and C_2H_6 both coincide well with the simulated breakthrough curves (Figure S14). During this time interval, 1.65 mmol g^{-1} of 99.9 % pure C_2H_4 can be

© 2022 Wiley-VCH GmbH

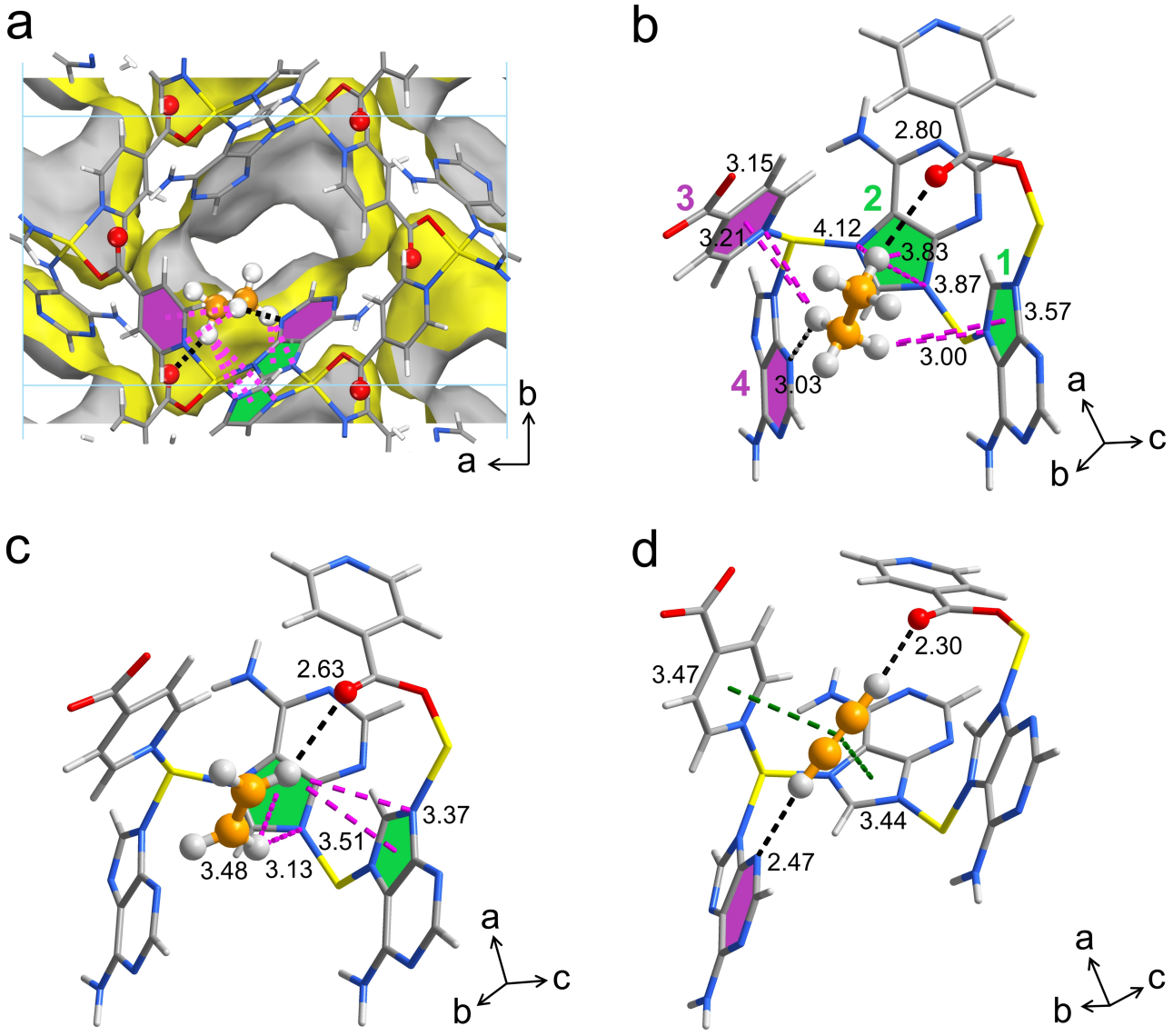

Figure 3. The refined structures of gas-loaded Zn(ad)(int). a) Adsorption site of C_2H_6 in Zn(ad)(int) obtained from in situ PXRD analyses and structural refinements. b)–d) Local environment showing the binding modes of C_2H_6, C_2H_4, and C_2H_2 in Zn(ad)(int). Black, green, and pink dash lines refer to hydrogen bonding, π···π stacking, and C–H···π interaction, respectively. All interatomic distances are in angstroms.

directly obtained, which is higher than Azole-Th-1 (1.13 mmol g^{-1}),[13h] $Fe_2(O_2)$(dobdc) (0.79 mmol g^{-1}),[14] and MAF-49 (0.28 mmol g^{-1}),[6c] the latter two of which are top-performing materials for inverse C_2H_6/C_2H_4 separation. In the separation of C_2H_6/C_2H_4 (50/50) mixture (Figure 4c), the material also exhibits desirable performance with 0.32 mmol g^{-1} of C_2H_4 (99.9 %) directly produced. Importantly, in the separation of ternary $C_2H_2/C_2H_6/C_2H_4$ (1/10/89) mixture (Figure 4d), the much later breakthrough times of C_2H_2 and C_2H_6 (46 and 56 min) than that of C_2H_4 (31 min) indicate that highly efficient trap of C_2H_2 and C_2H_6 can be simultaneously realized by Zn(ad)(int). The productivity of 99.9 % pure C_2H_4 harvested from the ternary mixture before the elution of C_2H_2 and C_2H_6 can be 1.43 mmol g^{-1}, which outperforms the best-performing C_2H_2/C_2H_6-selective materials Azole-Th-1 (1.34 mmol g^{-1}, 1/9/90)[13h] and TJT-100 (0.69 mmol g^{-1}, 0.5/0.5/99),[2] and sets a new benchmark. In cyclic breakthrough tests (Figure S16), Zn(ad)(int) well maintains its excellent separation performance with the breakthrough times of C_2H_2, C_2H_6, and C_2H_4 being almost unchanged within five cycles. PXRD and FTIR analyses also suggest that the material is highly stable and can be repeatedly used (Figure S1 and S17). These phenomena verify that Zn(ad)(int), which can be produced at an estimated low cost of ≈$60 kg^{-1}, is a promising adsorbent for the energy-efficient and one-step C_2H_4 purification.

Conclusion

In this work, we report the one-step purification of C_2H_4 from a ternary C2 hydrocarbon mixture by a MOF Zn(ad)-

© 2022 Wiley-VCH GmbH

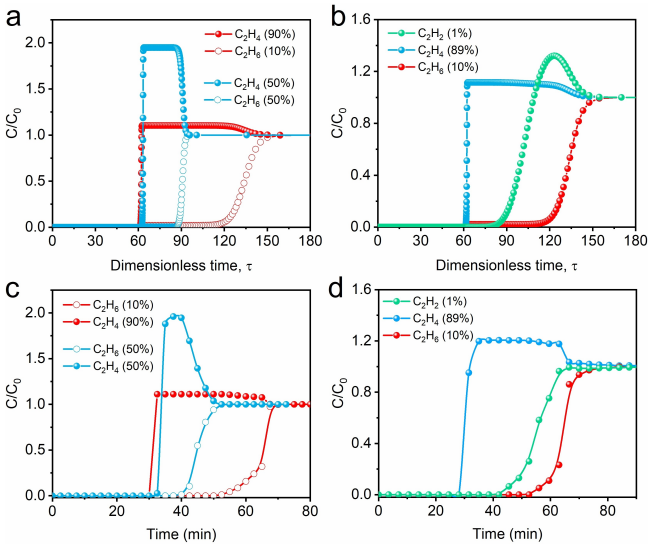

Figure 4. Simulated transient breakthrough curves and experimental dynamic breakthrough curves. a), b) Simulated transient breakthrough curves for the separation of C_2H_6/C_2H_4 (10/90 and 50/50) and $C_2H_2/C_2H_6/C_2H_4$ (1/10/89) mixtures on Zn(ad)(int) at 298 K. c), d) Experimental breakthrough curves for the separation of C_2H_6/C_2H_4 (10/90 and 50/50) and $C_2H_2/C_2H_6/C_2H_4$ (1/10/89) mixtures on Zn(ad)(int) at 298 K with a gas flow rate of 2 mL min^{-1}.

(int) with customized pore chemistry and shape. The combination of dual functional sites (dense heterocyclic rings and partially coordinated carboxyl groups) with interesting shape matching in the spindle-like molecular cage gives the material a dramatic ability to simultaneously capture C_2H_2 and C_2H_6, which is confirmed by in situ PXRD and FTIR analyses. Zn(ad)(int) exhibits not only high separation selectivities for C_2H_2/C_2H_4 and C_2H_6/C_2H_4 (1.61 and 2.4), but also excellent trapping abilities towards C_2H_2 and C_2H_6. Direct production of polymer-grade C_2H_4 from a ternary $C_2H_2/C_2H_6/C_2H_4$ mixture with a high productivity (1.43 mmol g^{-1}) was realized in breakthrough experiments, suggesting Zn(ad)(int) as a top-performing C_2H_2/C_2H_6-selective material. This work not only provides a novel microporous material with an impressive performance for C_2H_4 purification, but also affords important clues for the design of multifunctional materials towards the separation of complicated gas mixtures by pore environment control.

Acknowledgements

The authors acknowledge Agency for Science, Technology and Research of Singapore for LCER FI project with Award ID U2102d2009 for financial support.

Conflict of Interest

The authors declare no conflict of interest.

Data Availability Statement

The data that support the findings of this study are available in the Supporting Information of this article.

Keywords: Acetylene · Adsorptive Separation · C2 Hydrocarbon · Ethylene Purification · Inverse Adsorption

[1] a) R.-B. Lin, L. Li, H.-L. Zhou, H. Wu, C. He, S. Li, R. Krishna, J. Li, W. Zhou, B. Chen, *Nat. Mater.* **2018**, *17*, 1128–1133; b) K.-J. Chen, D. G. Madden, S. Mukherjee, T. Pham, K. A. Forrest, A. Kumar, B. Space, J. Kong, Q.-Y. Zhang, M. J. Zaworotko, *Science* **2019**, *366*, 241–246.

[2] H.-G. Hao, Y.-F. Zhao, D.-M. Chen, J.-M. Yu, K. Tan, S. Ma, Y. Chabal, Z.-M. Zhang, J.-M. Dou, Z.-H. Xiao, G. Day, H.-C. Zhou, T.-B. Lu, *Angew. Chem. Int. Ed.* **2018**, *57*, 16067–16071; *Angew. Chem.* **2018**, *130*, 16299–16303.

[3] Z. Bao, J. Wang, Z. Zhang, H. Xing, Q. Yang, Y. Yang, H. Wu, R. Krishna, W. Zhou, B. Chen, Q. Ren, *Angew. Chem. Int. Ed.* **2018**, *57*, 16020–16025; *Angew. Chem.* **2018**, *130*, 16252–16257.

[4] D. S. Sholl, R. P. Lively, *Nature* **2016**, *532*, 435–437.

[5] a) H. Wang, X. Dong, V. Colombo, Q. Wang, Y. Liu, W. Liu, X. Wang, X. Huang, D. M. Proserpio, A. Sironi, Y. Han, J. Li, *Adv. Mater.* **2018**, *30*, 1805088; b) J.-R. Li, J. Sculley, H.-C. Zhou, *Chem. Rev.* **2012**, *112*, 869–932; c) J. Shang, G. Li, R. Singh, Q. Gu, K. M. Nairn, T. J. Bastow, N. Medhekar, C. M. Doherty, A. J. Hill, J. Z. Liu, P. A. Webley, *J. Am. Chem. Soc.* **2012**, *134*, 19246–19253; d) H. Zeng, M. Xie, T. Wang, R.-J. Wei, X.-J. Xie, Y. Zhao, W. Lu, D. Li, *Nature* **2021**, *595*, 542–548; e) P.-Q. Liao, N.-Y. Huang, W.-X. Zhang, J.-P. Zhang, X.-M. Chen, *Science* **2017**, *356*, 1193–1196.

[6] a) Z. Zhang, S. B. Peh, Y. Wang, C. Kang, W. Fan, D. Zhao, *Angew. Chem. Int. Ed.* **2020**, *59*, 18927–18932; *Angew. Chem.* **2020**, *132*, 19089–19094; b) S. Yang, A. J. Ramirez-Cuesta, R. Newby, V. Garcia-Sakai, P. Manuel, S. K. Callear, S. I. Campbell, C. C. Tang, M. Schröder, *Nat. Chem.* **2015**, *7*, 121–129; c) P.-Q. Liao, W.-X. Zhang, J.-P. Zhang, X.-M. Chen, *Nat. Commun.* **2015**, *6*, 8697; d) C. Gu, N. Hosono, J. Zheng, Y. Sato, S. Kusaka, S. Sakaki, S. Kitagawa, *Science* **2019**, *363*, 387–391; e) Q. Ding, Z. Zhang, C. Yu, P. Zhang, J. Wang, X. Cui, C.-H. He, S. Deng, H. Xing, *Sci. Adv.* **2020**, *6*, eaaz4322.

[7] a) C. He, Y. Wang, Y. Chen, X. Wang, J. Yang, L. Li, J. Li, *ACS Appl. Mater. Interfaces* **2020**, *12*, 52819–52825; b) L. Jiang, Y. Tian, T. Sun, Y. Zhu, H. Ren, X. Zou, Y. Ma, K. R. Meihaus, J. R. Long, G. Zhu, *J. Am. Chem. Soc.* **2018**, *140*, 15724–15730.

[8] a) Y. Liu, Y. Wu, W. Liang, J. Peng, Z. Li, H. Wang, M. J. Janik, J. Xiao, *Chem. Eng. Sci.* **2020**, *220*, 115636; b) P. J. Bereciartua, Á. Cantín, A. Corma, J. L. Jordá, M. Palomino, F. Rey, S. Valencia, E. W. Corcoran, P. Kortunov, P. I. Ravikovitch, A. Burton, C. Yoon, Y. Wang, C. Paur, J. Guzman, A. R. Bishop, G. L. Casty, *Science* **2017**, *358*, 1068–1071; c) Y. Chai, X. Han, W. Li, S. Liu, S. Yao, C. Wang, W. Shi, I. da-Silva, P. Manuel, Y. Cheng, L. D. Daemen, A. J. Ramirez-Cuesta, C. C. Tang, L. Jiang, S. Yang, N. Guan, L. Li, *Science* **2020**, *368*, 1002–1006.

[9] W. Liang, Y. Wu, H. Xiao, J. Xiao, Y. Li, Z. Li, *AIChE J.* **2018**, *64*, 3390–3399.

[10] K. Su, W. Wang, S. Du, C. Ji, D. Yuan, *Nat. Commun.* **2021**, *12*, 3703.

[11] a) B. Li, X. Cui, D. O'Nolan, H.-M. Wen, M. Jiang, R. Krishna, H. Wu, R.-B. Lin, Y.-S. Chen, D. Yuan, H. Xing, W. Zhou, Q. Ren, G. Qian, M. J. Zaworotko, B. Chen, *Adv. Mater.* **2017**, *29*, 1704210; b) Y.-L. Peng, T. Pham, P. Li, T. Wang, Y. Chen, K.-

© 2022 Wiley-VCH GmbH

J. Chen, K. A. Forrest, B. Space, P. Cheng, M. J. Zaworotko, Z. Zhang, *Angew. Chem. Int. Ed.* **2018**, *57*, 10971–10975; *Angew. Chem.* **2018**, *130*, 11137–11141; c) Y. Belmabkhout, Z. Zhang, K. Adil, P. M. Bhatt, A. Cadiau, V. Solovyeva, H. Xing, M. Eddaoudi, *Chem. Eng. J.* **2019**, *359*, 32–36; d) J. Wang, Y. Zhang, P. Zhang, J. Hu, R.-B. Lin, Q. Deng, Z. Zeng, H. Xing, S. Deng, B. Chen, *J. Am. Chem. Soc.* **2020**, *142*, 9744–9751; e) E. D. Bloch, W. L. Queen, R. Krishna, J. M. Zadrozny, C. M. Brown, J. R. Long, *Science* **2012**, *335*, 1606–1610; f) X. Cui, K. Chen, H. Xing, Q. Yang, R. Krishna, Z. Bao, H. Wu, W. Zhou, X. Dong, Y. Han, B. Li, Q. Ren, M. J. Zaworotko, B. Chen, *Science* **2016**, *353*, 141–144.

[12] a) M. Kang, S. Yoon, S. Ga, D. W. Kang, S. Han, J. H. Choe, H. Kim, D. W. Kim, Y. G. Chung, C. S. Hong, *Adv. Sci.* **2021**, *8*, 2004940; b) M. Kang, D. W. Kang, J. H. Choe, H. Kim, D. W. Kim, H. Park, C. S. Hong, *Chem. Mater.* **2021**, *33*, 6193–6199; c) J. Pei, J.-X. Wang, K. Shao, Y. Yang, Y. Cui, H. Wu, W. Zhou, B. Li, G. Qian, *J. Mater. Chem. A* **2020**, *8*, 3613–3620; d) R. Lin, H. Wu, L. Li, X. Tang, Z. Li, J. Gao, H. Cui, W. Zhou, B. Chen, *J. Am. Chem. Soc.* **2018**, *140*, 12940–12946.

[13] a) S.-Q. Yang, F.-Z. Sun, P. Liu, L. Li, R. Krishna, Y.-H. Zhang, Q. Li, L. Zhou, T.-L. Hu, *ACS Appl. Mater. Interfaces* **2021**, *13*, 962–969; b) Y. Wang, C. Hao, W. Fan, M. Fu, X. Wang, Z. Wang, Y. L. Lei Zhu, X. Lu, F. Dai, Z. Kang, R. Wang, W. Guo, S. Hu, D. Sun, *Angew. Chem. Int. Ed.* **2021**, *60*, 11350–11358; *Angew. Chem.* **2021**, *133*, 11451–11459; c) L. Fan, P. Zhou, X. Wang, L. Yue, L. Li, Y. He, *Inorg. Chem.* **2021**, *60*, 10819–10829; d) Z. Jiang, L. Fan, P. Zhou, T. Xu, S. Hu, J. Chen, D.-L. Chen, Y. He, *Inorg. Chem. Front.* **2021**, *8*, 1243–1252; e) X.-W. Gu, J.-X. Wang, E. Wu, H. Wu, W. Zhou, G. Qian, B. Chen, B. Li, *J. Am. Chem. Soc.* **2022**, *144*, 2614–2623; f) B. Zhu, J.-W. Cao, S. Mukherjee, T. Pham, T. Zhang, T. Wang, X. Jiang, K. A. Forrest, M. J. Zaworotko, K.-J. Chen, *J. Am. Chem. Soc.* **2021**, *143*, 1485–1492; g) J.-W. Cao, S. Mukherjee, T. Pham, Y. Wang, T. Wang, T. Zhang, X. Jiang, H.-J. Tang, K. A. Forrest, B. Space, M. J. Zaworotko, K.-J. Chen, *Nat. Commun.* **2021**, *12*, 6507; h) Z. Xu, X. Xiong, J. Xiong, R. Krishna, L. Li, Y. Fan, F. Luo, B. Chen, *Nat. Commun.* **2020**, *11*, 3163.

[14] L. Li, R.-B. Lin, R. Krishna, H. Li, S. Xiang, H. Wu, J. Li, W. Zhou, B. Chen, *Science* **2018**, *362*, 443–446.

[15] F. Wang, Y.-X. Tan, H. Yang, H.-X. Zhang, Y. Kang, J. Zhang, *Chem. Commun.* **2011**, *47*, 5828–5830.

[16] R. E. Sikma, N. Katyal, S.-K. Lee, J. W. Fryer, C. G. Romero, S. K. Emslie, E. L. Taylor, V. M. Lynch, J.-S. Chang, G. Henkelman, S. M. Humphrey, *J. Am. Chem. Soc.* **2021**, *143*, 13710–13720.

[17] M. Anioła, Z. Dega-Szafran, A. Katrusiak, A. Komasa, M. Szafran, *Vib. Spectrosc.* **2016**, *85*, 35–42.

[18] S. Thicoipe, P. Carbonniere, C. Pouchan, *Theor. Chem. Acc.* **2017**, *136*, 44.

Manuscript received: June 2, 2022
Accepted manuscript online: July 11, 2022
Version of record online: July 21, 2022

© 2022 Wiley-VCH GmbH

Supporting Information
©Wiley-VCH 2021
69451 Weinheim, Germany

One-step Ethylene Purification from Ternary Mixtures in a Metal–Organic Framework with Customized Pore Chemistry and Shape

Qi Ding,† Zhaoqiang Zhang,† Yulong Liu, Kungang Chai, Rajamani Krishna, and Sui Zhang*

Abstract: Adsorptive separation is an energy-efficient technology for the separation of C2 hydrocarbons. However, it remains a critical problem to directly produce high-purity C_2H_4 from ternary $C_2H_2/C_2H_4/C_2H_6$ mixtures by simultaneously trapping C_2H_2 and C_2H_6. Herein, we report the one-step C_2H_4 purification from the ternary mixture by a metal–organic framework Zn(ad)(int) (ad = adeninate; int = isonicotinate). The material well combines dense heterocyclic rings and accessible uncoordinated O atoms as strong binding sites for C_2H_6 and C_2H_2. Meanwhile, the featured spindle-like cage exhibits an interesting shape matching with the targeted molecules, affording Zn(ad)(int) not only high separation selectivity for C_2H_6/C_2H_4 and C_2H_2/C_2H_4, but also excellent gas capacity. Breakthrough experiments show that polymer-grade C_2H_4 can be separated from the ternary mixtures with a record productivity of 1.43 mmol g^{-1}. In-situ powder X-ray diffraction and Fourier transform infrared spectrum analyses further provide deep insights into the separation mechanism.

DOI: 10.1002/anie.202208134

SUPPORTING INFORMATION

Table of Contents

SUPPORTING INFORMATION

Experimental Procedures

Chemicals. Zinc nitrate hexahydrate (≥99.0%), adenine (≥99.0%), and isonicotinic acid (≥99.0%) were purchased from Sigma-Aldrich Co. Ltd. and used as received without any further purification.

Synthesis of Zn(ad)(int). Zn(ad)(int) was synthesized by a hydrothermal method[1]. A mixture containing 1 mmol of $Zn(NO_3)_2{\cdot}6H_2O$, 1 mmol of adenine, 1 mmol of isonicotinic acid, and 6 mL of DMF was poured into a Teflon tube, and heated at 120°C for three days. After naturally cooled to room temperature, the crystalline product was collected by filtration and washed with water and methanol. Then, the material was outgassed at 140°C for 12 h under high vacuum to produce Zn(ad)(int).

Adsorption isotherm measurement. The adsorption isotherms were measured on the instrument of Micromeritics ASAP 2460. Before each measurement, about 100 mg of Zn(ad)(int) was loaded into a glass analysis tube and heated at 140°C for 12 h under a high vacuum (< 7 μmHg). The sample was backfilled with N_2 before transferred to the analysis port, where it was evacuated for another 60 min before the analysis started.

Thermal gravimetric analyses. Thermal gravimetric analyses (TGA) were performed on a TA instruments STD-600 equipment at a heating rate of 10 ºC min^{-1} up to 800 ºC with N_2 flow rate of 20 mL min^{-1}. The sample holders were alumina crucibles and the amount of each sample used during the tests was 10 (± 2) mg.

Powder X-ray diffraction analyses. Powder X-ray diffraction (PXRD) patterns were collected using a Rigaku Miniflex 600 diffractometer (Cu Kα λ = 1.540598 Å) with an operating power of 40 kV, 15 mA and a scan rate of 2.0° min^{-1}. The data were collected in a two-theta range of 5–40°. In situ PXRD patterns were collected using a capillary tube packed with the sample, which was firstly evacuated, and then filled with the C2 gas. Rietveld structural refinements were performed on the obtained PXRD data using the Reflex Module in *Materials Studio* software (Accelrys Software Inc.). C–H···O/N hydrogen bonding interactions were identified with the criterion that the distance of H···O/N is less than 3.2 Å, and ∠C–H···O is larger than 110°[2]. C–H···π interactions were identified using the criterion that $d \leq 4.3$ Å; $\theta \leq 30°$; $\varphi \geq 120°$[3]. d refers to the distance between the donor carbon atom and the center of the acceptor ring; θ refers to the angle between the ring normal and a vector connecting the carbon atom and the center of the ring; φ refers to the angle between C–H bond and the ring center-H vectors.

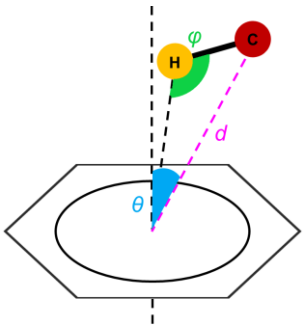

Fourier transform infrared spectroscopy. The in situ Fourier transform infrared (FTIR) spectra were recorded using a FTIR spectrometer (Bruker VERTEX70-FTIR). Prior to each test, the sample (ca. 100 mg) was pretreated under high vacuum condition (< 3 μmHg) at 140°C for 6 h to remove the moisture, and then cooled to room temperature. The sample was then exposed to C2 hydrocarbons with a pressure of 1.0 bar for 24 h to make sure that the adsorption has reached equilibrium. Then, the sample was used for FTIR test. All the spectra were recorded over accumulative 32 scans with a resolution of 4 cm^{-1} in the range of 4000–400 cm^{-1}.

Breakthrough experiment. The breakthrough expe140riments were conducted on a home-built dynamic gas breakthrough equipment. In a typical procedure, a stainless-steel column (Φ 4.6 × 100 mm) packed with 1.01 g of Zn(ad)(int) was firstly activated by a purge with a flow of N_2 gas (10 mL min^{-1}) at 140°C for 12 h. Hydrocarbon mixture (C_2H_6/C_2H_4 or $C_2H_2/C_2H_6/C_2H_4$ mixture) was then introduced into the column at a rate of 2 mL min^{-1} under 298 K and 1 bar. The concentration of the gas eluted from the outlet was detected by chromatography (GC-2018, SHIMADZU) with the thermal conductivity detector TCD. After the breakthrough experiment, the column was regenerated by a purge with N_2 at 140°C. The productivity of C_2H_4 was calculated by integrating the breakthrough curve area[4].

Breakthrough simulations. Transient breakthrough simulations were carried out at a total pressure of 100 kPa and temperature of 298 K, using the methodology described in earlier publications[5]. In the simulations, the intra-crystalline diffusion influences are considered to be negligible. For an adsorber of length, L, cross-sectional area, A, voidage of the packed bed, $\mathcal{E}$, the volume of MOF is $V_{ads} = LA(1\text{-}\mathcal{E})$ m^3. It is important to note that the volume of adsorbent, V_{ads}, includes the pore volume of the adsorbent material. If ρ is the crystal framework density, the mass of the adsorbent in the bed is $m_{ads} = (1\text{-}\mathcal{E}) \times (L \text{ m}) \times (A \text{ m}^2) \times (\rho \text{ kg m}^{-3})$ kg. The interstitial gas velocity in the bed, $v = u/\mathcal{E}$ where u is the superficial gas velocity at the inlet to the fixed bed. For comparison of breakthrough experiments with breakthrough simulations we use the same tube dimensions as in the experiments (Φ 4.6 × 100 mm). The

breakthrough simulation results are also presented in terms of a dimensionless time, $\tau = tv/L$, defined by dividing the actual time, t, by the characteristic time, L/v.

Calculation of IAST selectivity. The adsorption isotherms of C_2H_2, C_2H_4, and C_2H_6 were fitted using a single-site Langmuir model (1)

$$n = q_{sat}\frac{bp}{1+bp} \quad (1)$$

Here, p is the pressure of the bulk gas at equilibrium with the adsorbed phase (kPa), n is the adsorbed amount per mass of adsorbent (mmol g^{-1}), q_{sat} is the saturation capacity (mmol g^{-1}), b is the affinity coefficient (kPa^{-1}).

The adsorption selectivity is further calculated by the following equation (2)

$$S_{ads} = \frac{n_1/n_2}{p_1/p_2} \quad (2)$$

n_1 and n_2 are the molar loadings in the adsorbed phase in equilibrium with the bulk gas phase with partial pressures p_1 and p_2.

Calculation of Q_{st}. Q_{st} profiles for C_2H_2, C_2H_4, and C_2H_6 were derived from adsorption isotherms measured at 273, 298, and 313 K by Virial fitting method and Clausius-Claperyron equation.

A Virial-type expression (3) was used, where p represents the pressure in mmHg, n represents the gas uptake in mg g^{-1}, T represents the temperature in Kelvin, a_i and b_i are Virial coefficients independent of temperature, c and d are the numbers of coefficients required to adequately describe the isotherms.

$$\ln p = \ln n + \frac{1}{T}\sum_{i=0}^{c} a_i n^i + \sum_{j=0}^{d} b_i n^j \quad (3)$$

The isosteric heat of adsorption is calculated according to the following equation (4) derived from Clausius-Claperyron equation:

$$Q_{st} = -R\left[\frac{\partial \ln p}{\partial\left(\frac{1}{T}\right)}\right]_n = -R\sum_{i=0}^{m} a_i n^i \quad (4)$$

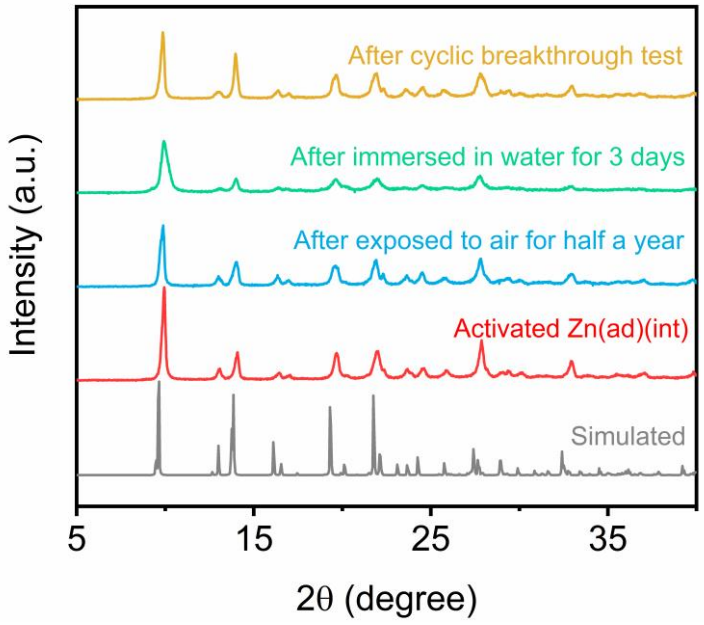

Figure S1. Simulated PXRD pattern of Zn(ad)(int), and the experimental PXRD patterns of Zn(ad)(int) after different treatments.

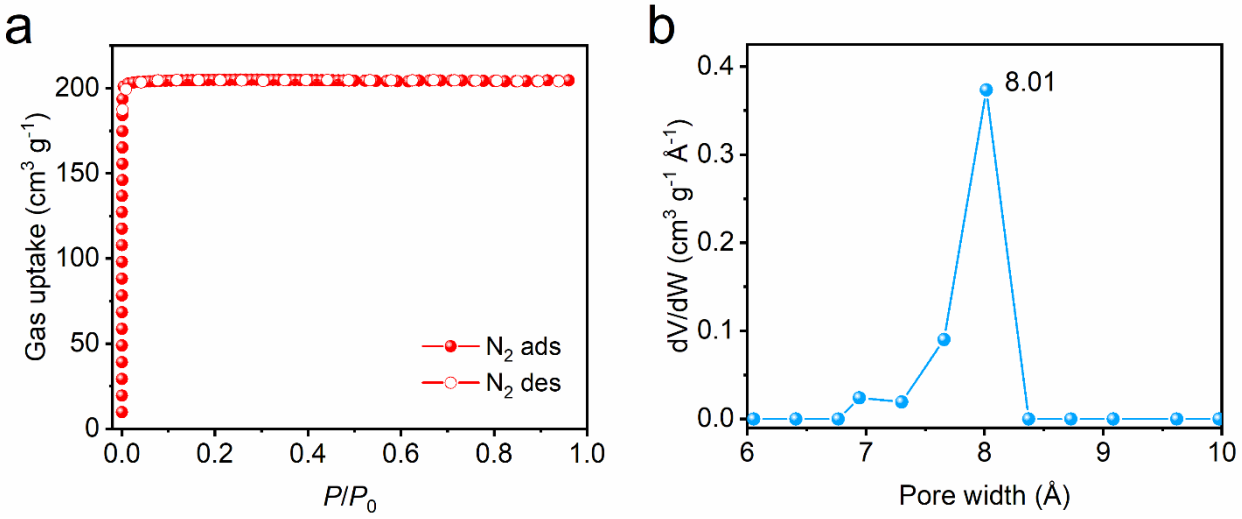

Figure S2. (a) Adsorption and desorption isotherms of N_2 on Zn(ad)(int) at 77 K. (b) Pore size distribution of Zn(ad)(int) derived from the N_2 adsorption isotherm by NLDFT model.

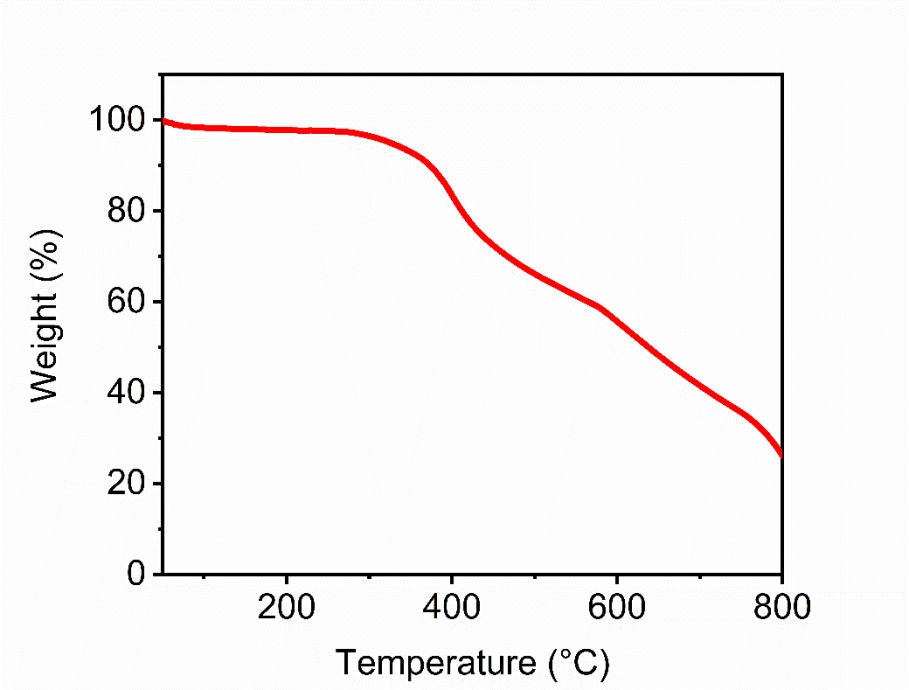

Figure S3. TGA curve of Zn(ad)(int).

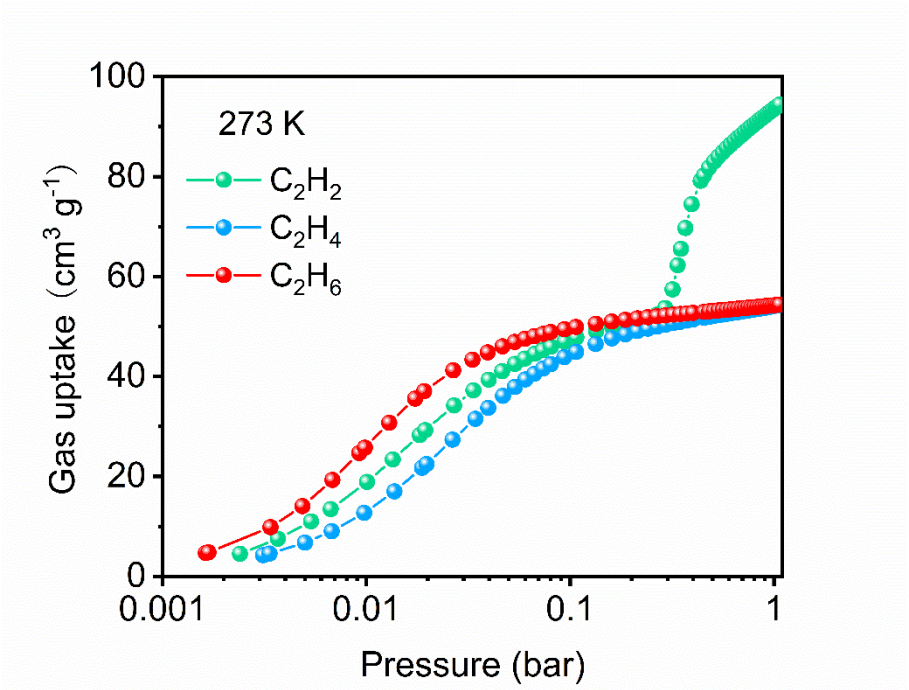

Figure S4. Adsorption isotherms of C_2H_2, C_2H_4, and C_2H_6 on Zn(ad)(int) at 273 K.

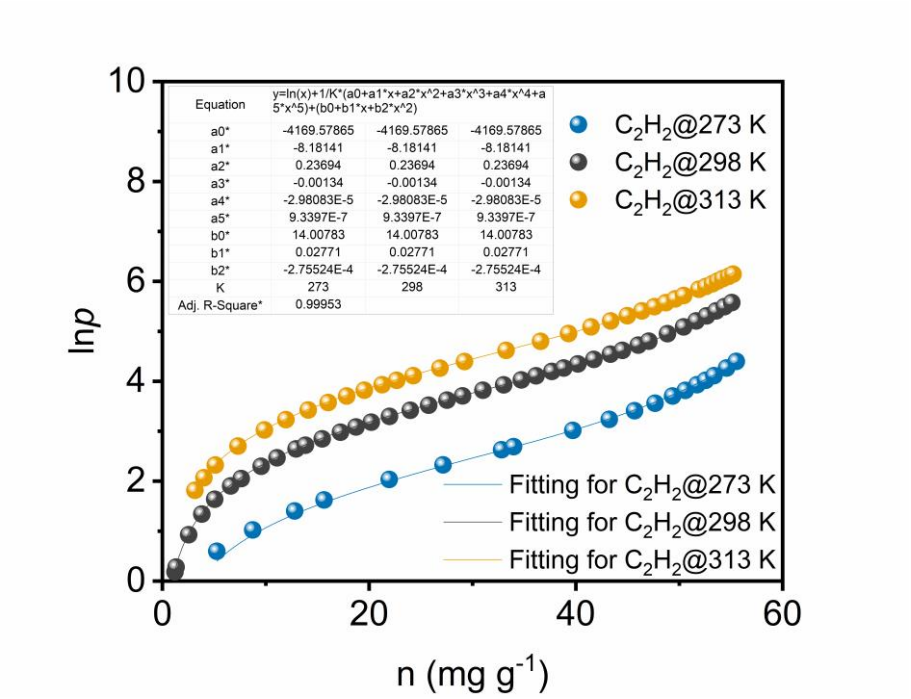

Figure S5. Virial fitting for the adsorption isotherms of C_2H_2 at different temperatures.

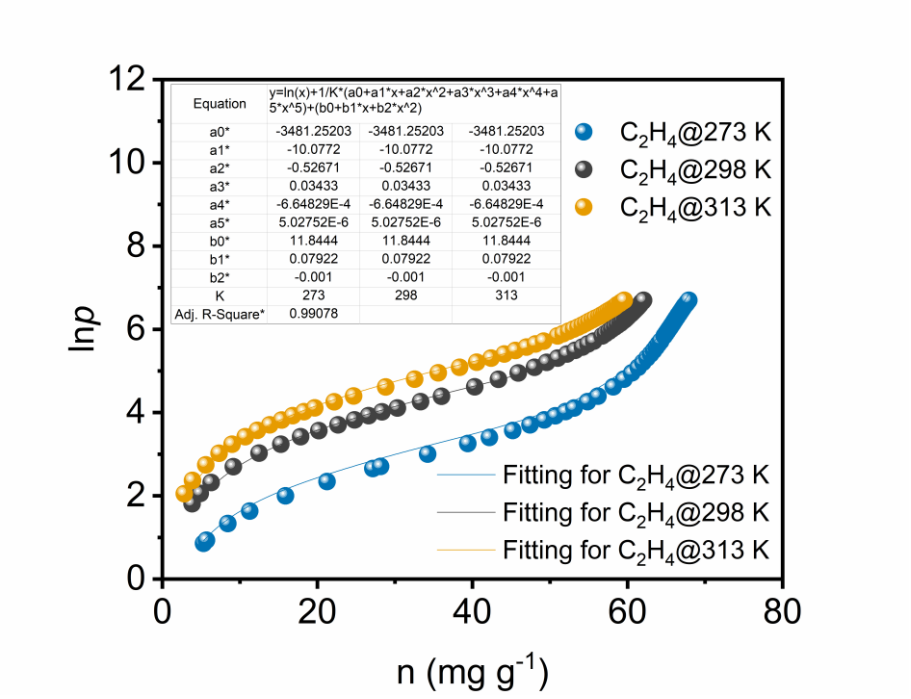

Figure S6. Virial fitting for the adsorption isotherms of C_2H_4 at different temperatures.

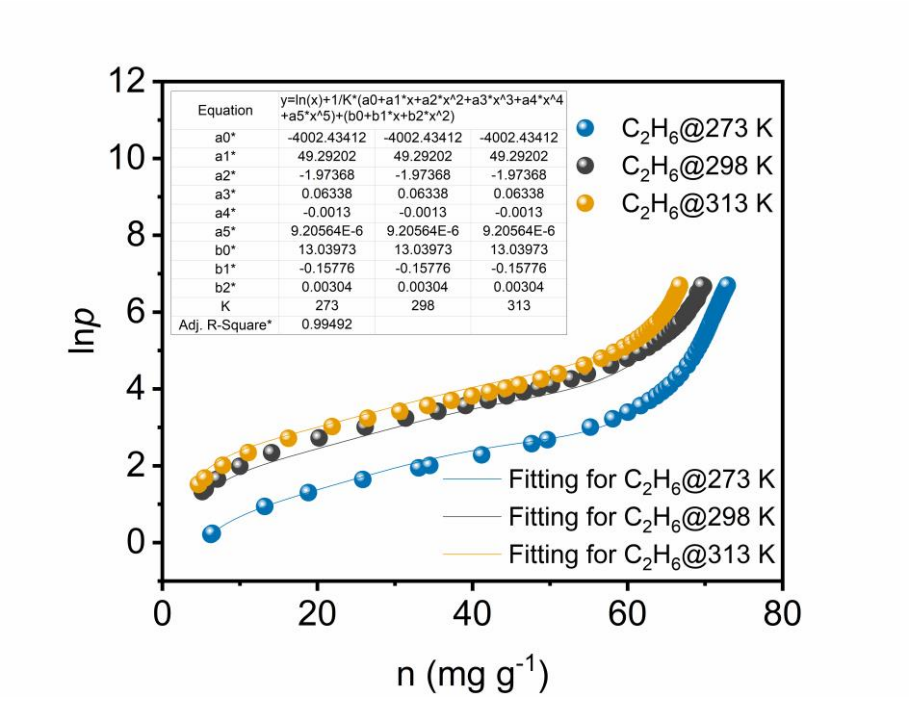

Figure S7. Virial fitting for the adsorption isotherms of C_2H_6 at different temperatures.

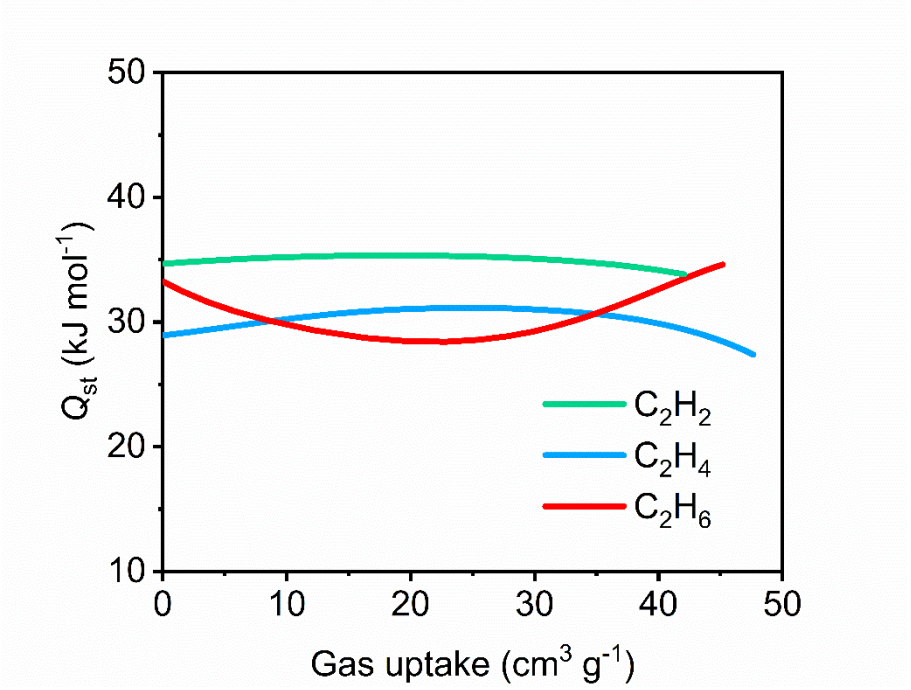

Figure S8. Q_{st} profiles of C_2H_2, C_2H_4, and C_2H_6 on Zn(ad)(int).

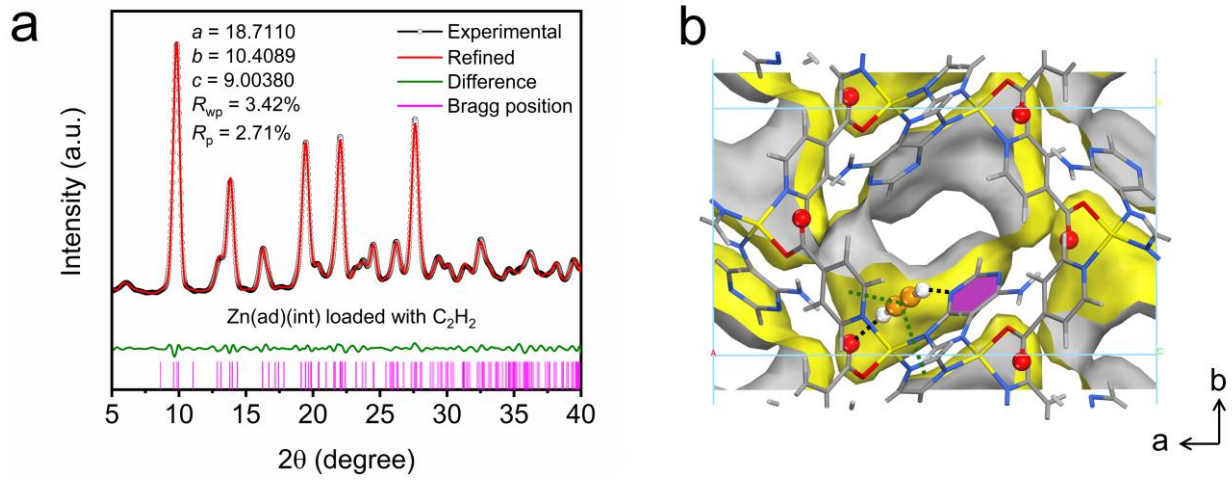

Figure S9. (a) Experimental in situ PXRD pattern (black circle) and refined PXRD pattern (red line) of Zn(ad)(int) loaded with C_2H_2. (b) Refined binding site of C_2H_2 in Zn(ad)(int).

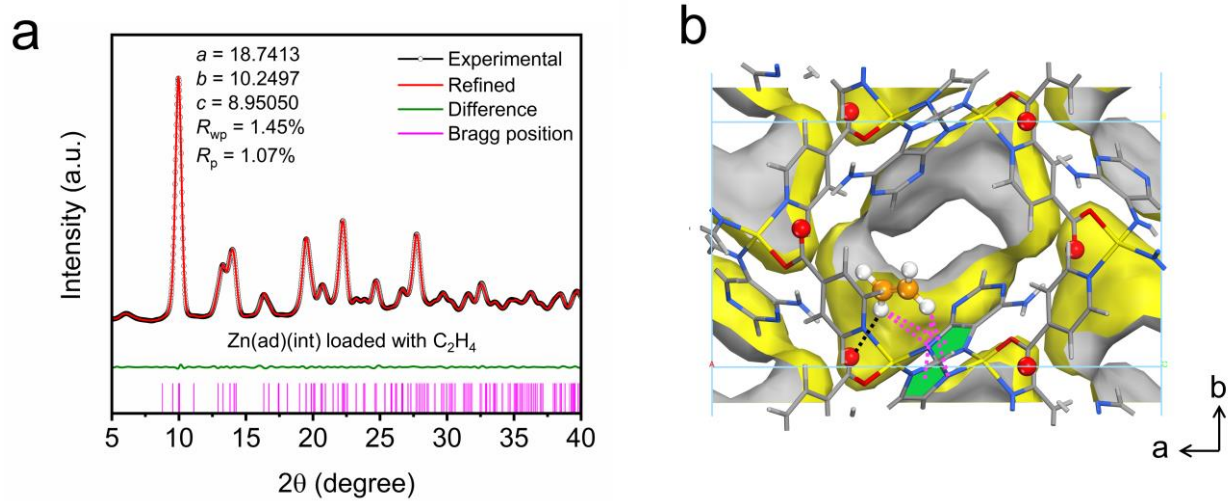

Figure S10. (a) Experimental in situ PXRD pattern (black circle) and refined PXRD pattern (red line) of Zn(ad)(int) loaded with C_2H_4. (b) Refined binding site of C_2H_4 in Zn(ad)(int).

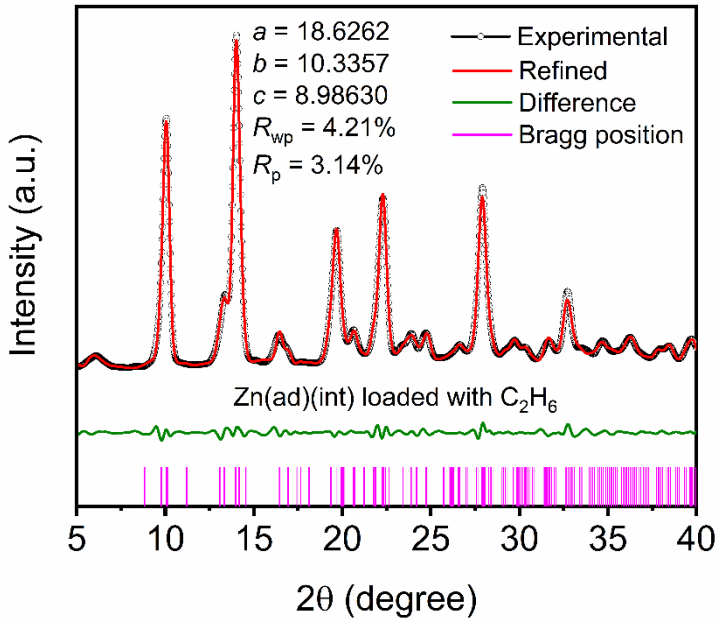

Figure S11. Experimental in situ PXRD pattern (black circle) and refined PXRD pattern (red line) of Zn(ad)(int) loaded with C_2H_6.

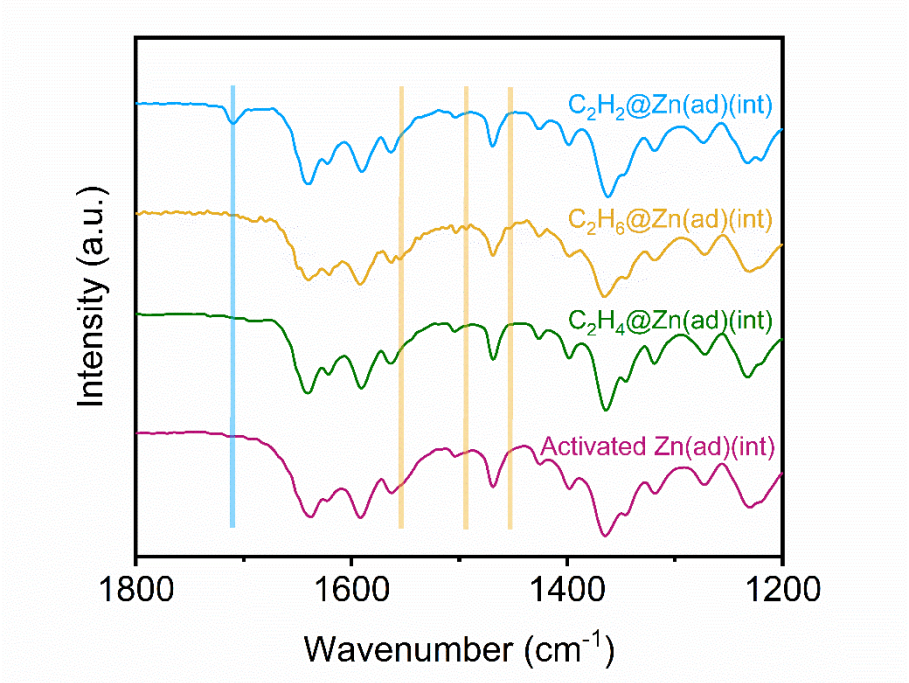

Figure S12. FTIR spectrums of Zn(ad)(int), and gas-loaded Zn(ad)(int).

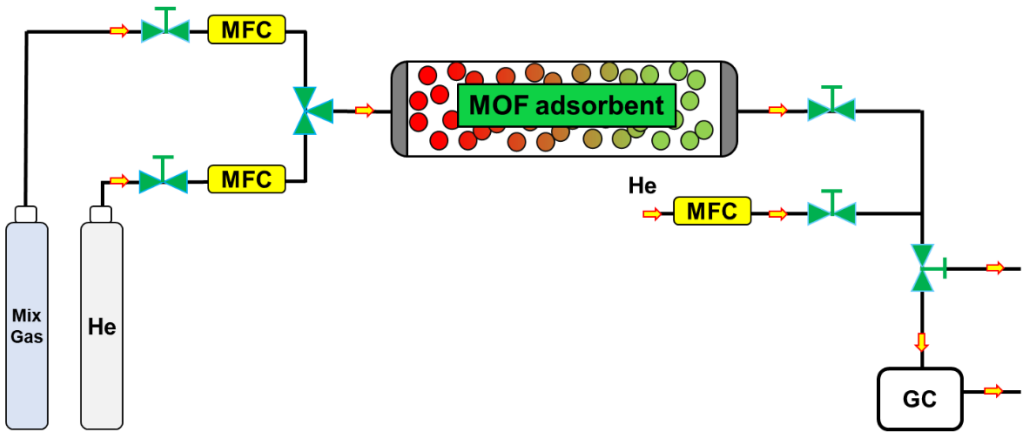

Figure S13. Scheme illustration for the breakthrough setup used in this study.

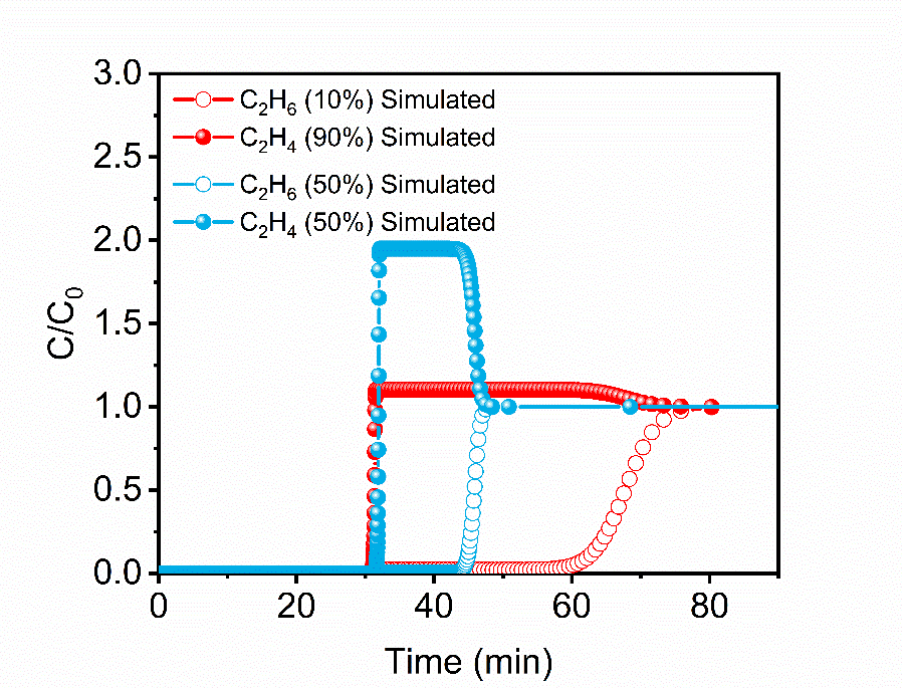

Figure S14. Simulated breakthrough curves for the separation of C_2H_6/C_2H_4 (10/90, 50/50) mixtures on Zn(ad)(int) material at 298 K with a gas flow rate of 2 mL min^{-1}.

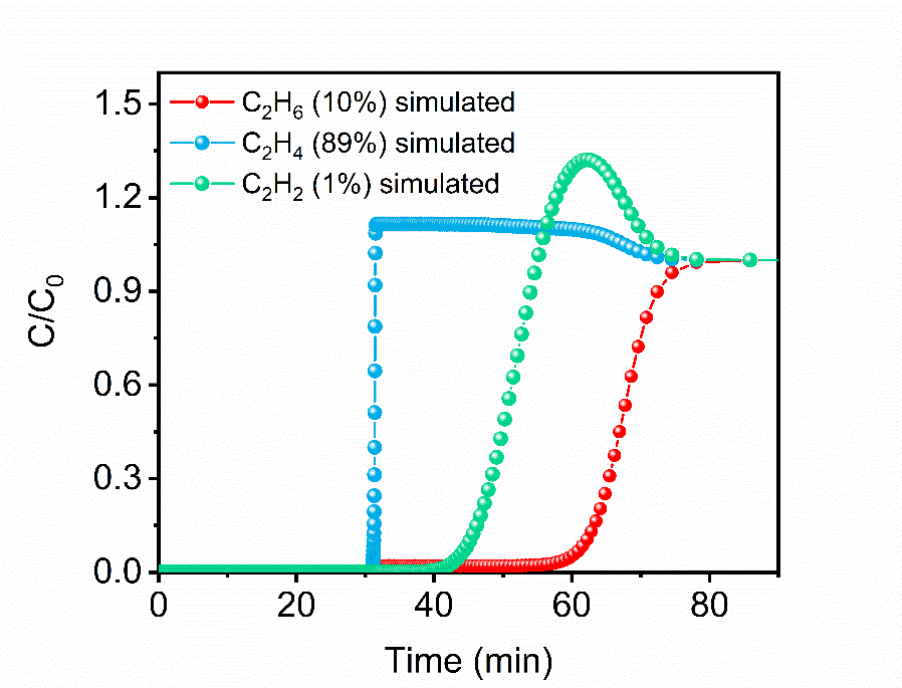

Figure S15. Simulated breakthrough curves for the separation of $C_2H_2/C_2H_6/C_2H_4$ (1/10/89) mixture on Zn(ad)(int) material at 298 K with a gas flow rate of 2 mL min^{-1}.

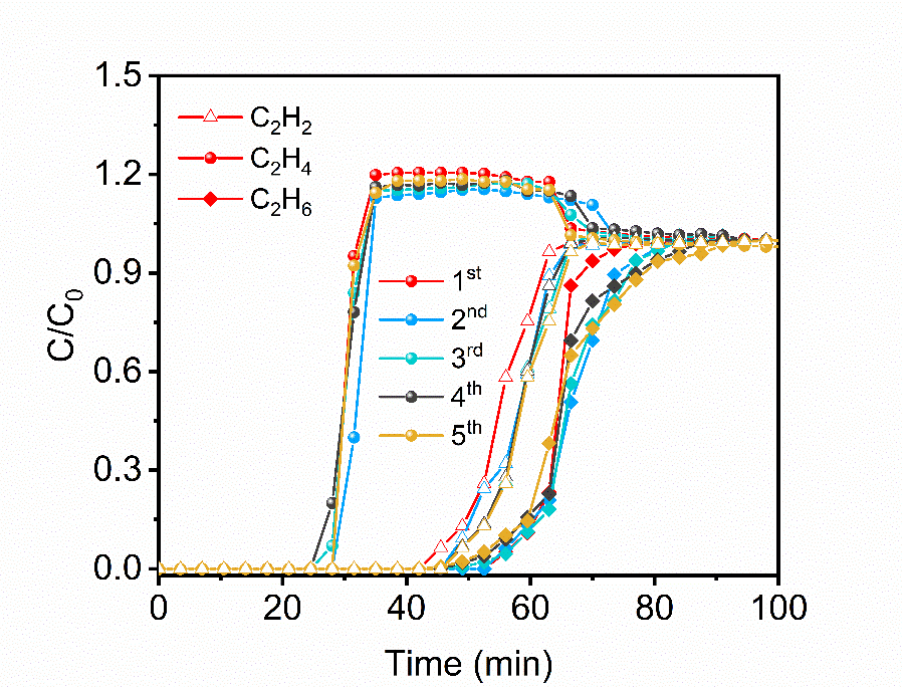

Figure S16. Cyclic breakthrough tests for the separation of $C_2H_2/C_2H_6/C_2H_4$ (1/10/89) mixture on Zn(ad)(int) material at 298 K with a gas flow rate of 2 mL min^{-1}.

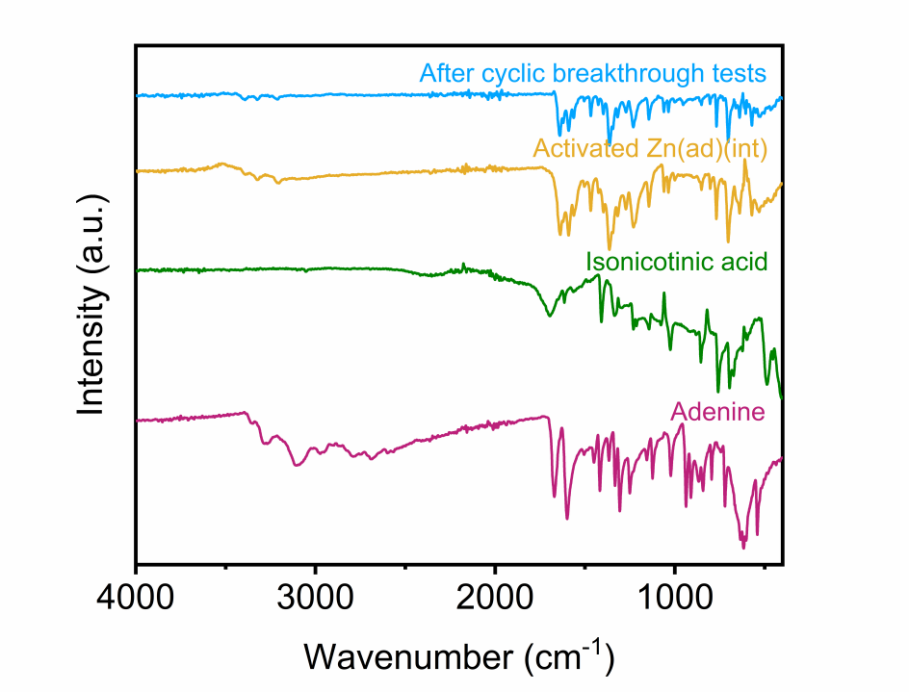

Figure S17. FTIR spectrums of isonicotinic acid, adenine, and Zn(ad)(int) before and after cyclic breakthrough tests.

Table S1. Properties of C_2H_2, C_2H_4, and C_2H_6

	C_2H_2	C_2H_4	C_2H_6
Boiling point (K)	188.4	169.4	184.5
Three-dimensional size ($Å^3$)	3.32×3.34×5.70	3.28×4.18×4.84	3.81×4.08×4.82
pK_a	26	45	62
Quadrupole moment ($\times 10^{-26}$ esu cm^2)	3.0	1.5	0.65
Polarizability ($\times 10^{-25}$ cm^3)	33.3–33.9	42.5	44.3–44.7

Table S2. Langmuir fitting parameters of C2 hydrocarbons on Zn(ad)(int) at 298 K

	C_2H_2	C_2H_4	C_2H_6
q_{sat} (mmol g^{-1})	2.569	2.461	2.444
b (kPa^{-1})	0.142	0.097	0.238
R^2	0.999	0.997	0.994

Table S3. A summary for the performance of materials reported for ternary C2 hydrocarbon separation

	C_2H_6 uptake (mmol g^{-1})		IAST selectivity			Q_{st} for C_2H_6 (kJ mol^{-1})	99.9% C_2H_4 recovered from $C_2H_2/C_2H_6/C_2H_4$ mixture (mmol g^{-1})	Temperature (K)	Reference
	0.1 bar	1 bar	C_2H_6/C_2H_4 10/90	C_2H_6/C_2H_4 50/50	C_2H_2/C_2H_4 1/99				
Zn(ad)(int)	1.83	2.32	2.4	2.4	1.61	33	1.43 (1/10/89)	298	This work
TJT-100	1.21	4.71	1.2[a]	/	1.8	29	0.69 (0.5/0.5/99)	298	[6]
Azole-Th-1	0.85	4.5	1.44	1.46	1.09[b]	28.6	1.34 (1/9/90)	298	[7]
NPU-1	1.30	4.5	/	1.32	1.4[b]	29.1	/	298	[8]
NPU-2	0.54	4.44	/	1.52	1.25[b]	19.64	/	298	[8]
NPU-3	0.34	3.36	/	3.21	1.32[b]	18.71	/	298	[8]
NUM-9a	1.07	2.48	1.62	1.61	1.48	35.75	/	298	[9]
ZJNU-7	1.38	4.13	1.56	1.58	1.77	29.7	/	298	[10]
Zn-atz-oba	0.64	2.05	/	1.27	1.43[b]	30.0	/	298	[11]
UiO-67-$(NH_2)_2$	1.10	5.32	/	1.7	2.1	26.5	0.55 (1/49.5/49.5)	296	[12]
UPC-612	0.45	3.58	1.4	1.4	1.1[c]	22.4	0.47 (1/1/1)	298	[13]
UPC-613	0.67	2.55	1.5	1.5	1.4[c]	31.8	0.34 (1/1/1)	298	[13]
ZJNU-115	1.07	4.21	/	1.56	2.05	28.2	/	298	[14]
Ag-PCM-102	1.1	3.7	/	/	1.5	/	/	303	[15]
CPOC-301	0.94	3.88	/	1.3	/	32.4	/	293	[16]

[a] IAST selectivity for 1/99 C_2H_6/C_2H_4 mixture

[b] IAST selectivity for 50/50 C_2H_2/C_2H_4 mixture

[c] IAST selectivity for 10/90 C_2H_2/C_2H_4 mixture

References

[1] F. Wang, Y.-X. Tan, H. Yang, H.-X. Zhang, Y. Kang, J. Zhang, *Chem. Commun.* **2011**, *47*, 5828-5830.
[2] J. L. Dragelj, G. V. Janjić, D. Ž. Veljković, S. D. Zarić, *Cryst. Eng. Comm.* **2013**, *15*, 10481-10489.
[3] a) M. J. Plevin, D. L. Bryce, J. Boisbouvier, *Nat. Chem.* **2010**, *2*, 466-471; b) H. Kaur, G. P. S. Raghava, *In. Silico. Biology* **2006**, *6*, 111-125.
[4] K.-J. Chen, D. G. Madden, S. Mukherjee, T. Pham, K. A. Forrest, A. Kumar, B. Space, J. Kong, Q.-Y. Zhang, M. J. Zaworotko, *Science* **2019**, *366*, 241-246.
[5] a) R. Krishna, *Sep. Purif. Technol.* **2018**, *194*, 281-300; b) R. Krishna, *RSC Adv.* **2017**, *7*, 35724-35737; c) R. Krishna, *RSC Adv.* **2015**, *5*, 52269-52295; d) R. Krishna, *Micropor. Mesopor. Mat.* **2014**, *185*, 30-50; e) R. Krishna, *ACS Omega* **2020**, *5*, 16987-17004.
[6] H.-G. Hao, Y.-F. Zhao, D.-M. Chen, J.-M. Yu, K. Tan, S. Ma, Y. Chabal, Z.-M. Zhang, J.-M. Dou, Z.-H. Xiao, G. Day, H.-C. Zhou, T.-B. Lu, *Angew. Chem. Int. Ed.* **2018**, *57*, 16067-16071.
[7] Z. Xu, X. Xiong, J. Xiong, R. Krishna, L. Li, Y. Fan, F. Luo, B. Chen, *Nat. Commun.* **2020**, *11*, 3163.
[8] B. Zhu, J.-W. Cao, S. Mukherjee, T. Pham, T. Zhang, T. Wang, X. Jiang, K. A. Forrest, M. J. Zaworotko, K.-J. Chen, *J. Am. Chem. Soc.* **2021**, *143*, 1485-1492.
[9] S.-Q. Yang, F.-Z. Sun, P. Liu, L. Li, R. Krishna, Y.-H. Zhang, Q. Li, L. Zhou, T.-L. Hu, *ACS Appl. Mater. Interfaces* **2021**, *13*, 962-969.
[10] Z. Jiang, L. Fan, P. Zhou, T. Xu, S. Hu, J. Chen, D.-L. Chen, Y. He, *Inorg. Chem. Front.* **2021**, *8*, 1243-1252.
[11] J.-W. Cao, S. Mukherjee, T. Pham, Y. Wang, T. Wang, T. Zhang, X. Jiang, H.-J. Tang, K. A. Forrest, B. Space, M. J. Zaworotko, K.-J. Chen, *Nat. Commun.* **2021**, *12*, 6507.
[12] X.-W. Gu, J.-X. Wang, E. Wu, H. Wu, W. Zhou, G. Qian, B. Chen, B. Li, *J. Am. Chem. Soc.* **2022**, *144*, 2614-2623.
[13] Y. Wang, C. Hao, W. Fan, M. Fu, X. Wang, Z. Wang, Y. L. Lei Zhu, X. Lu, F. Dai, Z. Kang, R. Wang, W. Guo, S. Hu, D. Sun, *Angew. Chem. Int. Ed.* **2021**, *60*, 11350-11358.
[14] L. Fan, P. Zhou, X. Wang, L. Yue, L. Li, Y. He, *Inorg. Chem.* **2021**, *60*, 10819-10829.
[15] R. E. Sikma, N. Katyal, S.-K. Lee, J. W. Fryer, C. G. Romero, S. K. Emslie, E. L. Taylor, V. M. Lynch, J.-S. Chang, G. Henkelman, S. M. Humphrey, *J. Am. Chem. Soc.* **2021**, *143*, 13710-13720.
[16] K. Su, W. Wang, S. Du, C. Ji, D. Yuan, *Nat. Commun.* **2021**, *12*, 3703.

Author Contributions

Q.D. carried out the experimental work on synthesis, material characterization, and adsorption isotherm measurements. Z.Z. conducted in situ PXRD analyses, structural refinements, and in situ FTIR analyses. Y.L. and K.C. performed the breakthrough experiments and cyclic tests. K.R. performed the breakthrough simulations. S.Z. and Q.D. conceived the idea and analyzed the results. All authors contributed to the final version of the manuscript.